Biomaterials 51 (2015) 173–183

Contents lists available at ScienceDirect

Biomaterials

journal homepage: www.elsevier.com/locate/biomaterials

Enhanced osteointegration on tantalum-implanted polyetheretherketone surface with bone-like elastic modulus

Tao Lu [a, 1], Jin Wen [b, c, 1], Shi Qian [a], Huiliang Cao [a], Congqin Ning [a], Xiaoxia Pan [d], Xinquan Jiang [b, c, **], Xuanyong Liu [a, *], Paul K. Chu [e]

[a] State Key Laboratory of High Performance Ceramics and Superfine Microstructure, Shanghai Institute of Ceramics, Chinese Academy of Sciences, Shanghai 200050, PR China
[b] Department of Prosthodontics, College of Stomatology, Ninth People's Hospital, School of Medicine, Shanghai Jiaotong University, 639 Zhizaoju Road, Shanghai 200011, PR China
[c] Oral Bioengineering Lab, Shanghai Research Institute of Stomatology, Ninth People's Hospital Affiliated to Shanghai Jiao Tong University, School of Medicine, Shanghai Key Laboratory of Stomatology, 639 Zhizaoju Road, Shanghai 200011, PR China
[d] State Key Laboratory of Molecular Engineering of Polymers & Department of Macromolecular Science, Fudan University, Shanghai 200433, PR China
[e] Department of Physics and Materials Science, City University of Hong Kong, Tat Chee Avenue, Kowloon, Hong Kong, China

ARTICLE INFO

Article history:
Received 18 December 2014
Accepted 2 February 2015
Available online

Keywords:
Polyetheretherketone
Tantalum
Plasma immersion ion implantation
Elastic modulus
Osteointegration

ABSTRACT

Polyetheretherketone (PEEK) possesses a similar elastic modulus as bones but yet suffers from bio-inertness and poor osteogenesis. In this work, tantalum ions are implanted energetically into PEEK by plasma immersion ion implantation (PIII) to form Ta_2O_5 nanoparticles in the near surface. Nano-indentation reveals that the surface elastic modulus of the Ta ion implanted PEEK is closer to that of human cortical bones. *In vitro* cell adhesion, alkaline phosphatase activity, collagen secretion, extracellular matrix mineralization, and real-time PCR analyses disclose enhanced adhesion, proliferation, and osteogenic differentiation of rat bone mesenchymal stem cells (bMSCs) on the Ta-PIII modified PEEK. *In vivo* evaluation of the cortico-cancellous rat femur model by means of micro-CT, sequential fluorescent labeling, and histological analysis after 8 weeks confirms significantly improved osteointegration. The bone-like elastic modulus and modified surface topography of the Ta-PIII modified PEEK synergistically induce osteogenic differentiation of bMSCs and the surface-modified materials have large potential in dental and orthopedic implants.

1. Introduction

Dental and orthopedic implants are hard tissue substitutes for impaired human bones in case of trauma, diseases, and aging [1–3] and polyetheretherketone (PEEK) is a prime candidate to replace traditional metallic implants made of titanium and its alloys [4–6]. Despite the good biocompatibility, titanium possesses a large elastic modulus of over 100 GPa whereas PEEK has an elastic modulus of about 5 GPa that is closer to that of cortical bones [6]. As a result of the mismatched elasticity between PEEK and human bones, there are concerns of osteanabrosis and bone resorption caused by stress shielding [7]. Besides, degradation of the mechanical properties of metallic implants caused by corrosion can be avoided due to the well-known good chemical resistance of PEEK [4]. Unfortunately, in spite of the above attractive properties, PEEK is normally bioinert thus impeding osteointegration *in vivo* after implantation.

Tantalum (Ta) is a biocompatible metal with excellent strength and anticorrosion properties even in an acidic medium. The excellent anticorrosion properties of tantalum originate from the stable Ta_2O_5 protective film formed on the surface [8–10] and the biocompatibility of Ta has also been demonstrated [11–13]. However, its large elastic modulus of over 186 GPa and density of 16.6 g/cm^3 make direct clinical application difficult. Hence, there has been much effort in lowering the elastic modulus and weight of tantalum products. For instance, tantalum has been used as an alloying

* Corresponding author. State Key Laboratory of High Performance Ceramics and Superfine Microstructure, Shanghai Institute of Ceramics, Chinese Academy of Sciences, Shanghai 200050, China. Tel./fax: +86 21 52412409.
** Corresponding author. Department of Prosthodontics, Ninth People's Hospital affiliated to Shanghai Jiao Tong University, School of Medicine, Shanghai 200011, PR China. Tel.: +86 21 63135412; fax: +86 21 63136856.
E-mail addresses: xinquanjiang@aliyun.com (X. Jiang), xyliu@mail.sic.ac.cn (X. Liu).
[1] These authors contributed equally to this work.

http://dx.doi.org/10.1016/j.biomaterials.2015.02.018
0142-9612/

constituent in titanium or niobium to reduce the weight of implants while enhancing the biocompatibility [14,15] and porous tantalum scaffolds with a small elastic modulus (from 3 to 25 GPa) have been produced to meet the practical requirements [16–19]. Nevertheless, potential deformation of porous tantalum under high pressure limits its use as a load-bearing bone substitute.

During the healing process, the surface properties of the biomaterials play a crucial role in the cell–implant interactions at the implant/tissue interface [20,21]. In this respect, surface modification is an effective way to tailor the surface mechanical and biological properties while preserving the favorable bulk characteristics of the materials. Among the various surface modification techniques, plasma immersion ion implantation (PIII) is a non-line-of-sight method that is suitable for biomedical products [22,23]. By introducing certain elements and functional groups into the biomaterials, specific bio-functions can be achieved [24–26]. For instance, our recent work indicated that the *in vitro* osteogenic activity of PEEK and carbon-fiber-reinforced PEEK was enhanced by altering the surface nanostructure using PIII [27,28]. However, the relationship between the surface mechanical properties altered by PIII and corresponding biological effects is not well understood. It has been suggested that the heat produced on the atomic scale during PIII consolidates the coating and improves the adhesion between the coating and substrate [29,30]. With regard to polymers, the thermal effects, namely heat accumulation, can be magnified due to the poor thermal conductivity. Consequently, carbonization, crosslinking, fusion, and/or resolidification can occur on the polymer surface thereby altering the surface elastic modulus and hardness. Gas ion PIII has been shown to improve the elastic recovery of polymers like PEEK [31] and polytetrafluorethylene (PTFE) [24] but no similar studies have been conducted for metal ion PIII.

In this work, tantalum plasma immersion ion implantation (Ta-PIII) is performed under different conditions to modify PEEK to take advantage of the favorable properties of PEEK and tantalum. The osteogenic properties of the Ta-PIII modified PEEK are determined systematically using rat bone marrow mesenchymal stem cells (bMSCs) *in vitro* and the materials are also inserted into the rat femur bones for 8 weeks to evaluate osteointegration *in vivo*.

2. Materials and methods

2.1. Sample preparation

Biomedical grade polyetheretherketone (PEEK) was machined into samples with different dimensions. Square samples ($10 \times 10 \times 1$ mm^3) were used for surface characterization, ion release tests, and *in vitro* studies on 24-well tissue culture plates, square samples ($20 \times 20 \times 1$ mm^3) were used in the real-time PCR tests, and cylindrical samples ($\phi 2 \times 10$ mm^3) were used in the *in vivo* animal evaluation. The samples were polished on one side to a near mirror finish and ultrasonically cleaned in acetone, ethanol, and ultra-pure water prior to PIII. Tantalum was implanted into the samples using a filtered cathodic arc source housing a 99.99% pure tantalum rod with a diameter of 10 mm. Before PIII, the chamber was evacuated to a pressure of 5×10^{-3} Pa. To attain stable ionization of tantalum, argon (Ar) was introduced to the cathodic arc source at a flow rate of 5 sccm (standard cubic centimeter per minute). The PEEK samples were placed on a rotating sample stage connected to a high voltage. By applying a pulsed negative high voltage, tantalum ions were implanted and the sample stage was continuously rotated to obtain uniform ion implantation. Table 1 lists the important parameters and corresponding sample designations.

Table 1
Main conditions used in tantalum plasma immersion ion implantation.

	PEEK	Ta-30	Ta-120
Cathodic arc pulse duration (μs)	–	500	500
High voltage pulse duration (μs)	–	500	500
Pulsing frequency (Hz)	–	7	7
Implantation voltage (kV)	–	30	30
Implantation time (min)	–	30	120

2.2. Surface characterization

2.2.1. Surface structure and chemical characterization

The surface morphology was examined by field-emission scanning electron microscopy (FE-SEM, Hitachi S-4800, Japan) at different magnification without a conductive coating. The surface chemical states and elemental depth profiles were determined by X-ray photoelectron spectroscopy (XPS, Physical Electronic PHI 5802) equipped with a monochromatic Al K_α source in City University of Hong Kong. The Ta depth profiles were acquired by XPS in conjunction with argon ion bombardment at a sputtering rate of about 4 nm/min.

The surface elastic modulus and hardness were determined by nanoindentation (Nano Indenter G200, Agilent, USA). The indentation depth range was 20–100 nm and the elastic recovery curves were acquired at a loading of 1.3 mN. At least eight indents were made to improve the statistics.

2.2.2. Ion release

Two pieces of each sample were incubated in 5 mL of phosphate buffered saline (PBS 1 M, pH = 7.4) for 7, 14, 21, and 28 days at 37 °C without stirring. At a prescribed time, all the 5 mL solution was withdrawn and analyzed by inductively-coupled plasma atomic emission spectroscopy (ICP-AES, JY2000-2, France) to determine the amount of released tantalum. The withdrawn solution was replaced by the same volume of fresh PBS.

2.3. In vitro studies

2.3.1. Cell culturing

The rat bone mesenchymal stem cells (bMSCs: provided by Stem Cell Bank, Chinese Academy of Science, Shanghai, China) were isolated from the bone marrow. The bMSCs were cultured in the α-minimum essential medium (α-MEM, Gibto-BRL, USA) with 10% fetal bovine serum (FBS, Hyclone, USA), 1% antimicrobial of penicillin, and streptomycin at 37 °C in a humidified atmosphere of 5% CO_2. The α-MEM was refreshed every 3 days during cell culturing and the experiments were carried out with the bMSCs before passage five. All the samples were sterilized with 75% alcohol for 3 h and rinsed twice with sterile PBS before cell seeding.

2.3.2. Cell adhesion

The bMSCs were seeded onto the samples on a 24-well plate at a density of 5×10^4 cells per well. After culturing for 1, 3, and 24 h, the samples were taken out and put on another 24-well plate. The samples were rinsed twice with PBS and fixed with 3% glutaraldehyde overnight. Ethanol with different concentrations of 30, 50, 75, 90, 95, 100, and 100% v/v was used sequentially to dehydrate the samples for 10 min. The samples were dried and sputter coated with platinum before SEM observation (SEM, Hitachi S-3400, Japan).

2.3.3. Cell proliferation and viability

The alamarBlue™ (AbD Serotec Ltd, UK) assay was employed to quantitatively determine the cell proliferation and viability on the samples. The bMSCs were seeded on the samples (four replicates) on 24-well plates at a density of 2.5×10^4 cells per well. After 1, 4, and 7 days, the culture medium was replaced by 0.5 mL of the fresh medium with 5% alamarBlue™ in each well. After incubation for 4 h, 100 μL of the medium was transferred to a 96-well plate for measurement. The amount of reduced alamarBlue™ was determined on an enzyme-labeling instrument (BIO-TEK, ELX 800) at wavelengths of 570 nm and 600 nm. The operation and calculation of cell proliferation followed the instruction of the alamarBlue™ assay.

2.3.4. Alkaline phosphatase activity

The bMSCs were seeded on the samples (four replicates) on 24-well plates at a density of 1×10^4 cells per well (culturing for 7 days) or 0.5×10^4 cells per well (culturing for 14 days). In the quantitative alkaline phosphatase (*ALP*) assay, after culturing for 7 and 14 days, a Bio-Rad protein assay kit (Bio-Rad, USA) was employed to calculate the total protein content and the results were adjusted with a series of BSA (Sigma) standards by measuring the optical density (OD) values of the absorbance at 570 nm. After incubation with p-nitrophenyl phosphate (Sigma) at 37 °C for 30 min, the *ALP* activity was calculated and adjusted with a series of 4-Nitrophend NaOH (0.02 M) solutions by measuring the OD values at 405 nm. The *ALP* levels were normalized to the total protein content and described as μM/mg total proteins.

For *ALP* staining, the samples cultured for 7 or 14 days were rinsed twice with PBS, immersed in citrate buffered acetone for cell fixation for 30 s, and rinsed with ultra-pure water for 45 s. A mixture of naphthol AS-MX phosphate (Sigma–Aldrich) and fast blue RR salt (Sigma–Aldrich) was used in alkaline-dyeing. The samplers were dyed with the alkaline-dye mixture for 30 min and rinsed thoroughly with ultra-pure water for 2 min. Finally, the samples were immersed in Mayer's Hematoxylin Solution (Sigma–Aldrich) for 10 min and rinsed with ultra-pure water for 3 min. The stained specimens were observed by fluorescence microscopy (Olympus IX 71, Olympus, Japan).

2.3.5. Collagen secretion

Collagen secretion of the bMSCs on the samples was quantified using Sirius Red staining method. The bMSCs were seeded on the samples (four replicates) on 24-well plates at a density of 1×10^4 cells per well (cultured for 7 days) or

0.5×10^4 cells per well (cultured for 14 days). At a prescribed time, the samples were washed three times with PBS and fixed in 4% paraformaldehyde. Following three rinses in PBS, the samples were stained for collagen secretion using a 0.1% solution of Sirius Red (Sigma) in saturated picric acid for 18 h. After washing with 0.1 M acetic acid until no red color appeared, images were taken by fluorescence microscopy (Olympus IX 71, Olympus, Japan). In the quantitative analysis, the stain on the samples was eluted in 500 mL of the solution (0.2 M NaOH/methanol = 1:1). The optical density at 540 nm was measured on an enzyme-labeling instrument.

2.3.6. Extracellular matrix mineralization

The extracellular matrix (ECM) mineralization by bMSCs on the samples was evaluated using Alizarin Red staining method. The bMSCs were seeded on the samples (four replicates) on 24-well plates at a density of 1×10^4 cells per well (cultured for 7 days) or 0.5×10^4 cells per well (cultured for 14 days). At a prescribed time, the bMSCs were washed thrice with PBS and fixed in 75% ethanol for 1 h. The samples were stained with 40 mM Alizarin Red in distilled water (pH = 4.2) for 10 min at room temperature. Afterwards, the samples were washed with distilled water until no color appeared and pictures were taken by fluorescence microscopy (Olympus IX 71, Olympus, Japan). In the quantitative analysis, the stain was dissolved with 10% cetylpyridinium chloride in 10 mM sodium phosphate (pH = 7.0) and the absorbance was monitored at 630 nm.

2.3.7. Quantitative real-time PCR

The expression of osteogenesis-related genes was analyzed quantitatively by the real-time reverse-transcriptase polymerase chain reaction (real-time PCR). Three pieces of each sample were placed on the cell culture dish (6 cm diameter, Nunc, Denmark) and the bMSCs were seeded at a density of 1×10^5 cells per dish (cultured for 7 days) or 0.5×10^5 cells per dish (cultured for 14 days). The total RNA was extracted using TRIZOL reagent (Invitrogen, USA) and the complementary DNA (cDNA) was reverse-transcribed from 1 μg of total RNA using a PrimeScript I Strand cDNA Synthesis kit (TaKaRa) according to the manufacturer's protocols. The forward and reverse primers for different genes are listed in Table 2. The expression of selected genes, including Type I collagen (*COL-I*), runt-related transcription factor 2 (*Runx2*), bone morphogenetic protein 2 (*BMP-2*), alkaline phosphatase (*ALP*), osteocalcin (*OCN*), and osteopontin (*OPN*) were analyzed with β-actin as the housekeeping gene for normalization and relatively quantified using real-time PCR (LightCycler 480 Real-Time PCR System, Roche, USA) using the following procedures: denaturation at 95 °C for 30 s and 40 cycles of PCR (95 °C for 10 s and 60 °C for 20 s). Quantification of the gene expression was based on the CT (cycle threshold) values.

2.4. In vivo studies

2.4.1. Surgical procedures

All the animal procedures and experiments were approved by the Animal Ethical Committee at the Ninth People's Hospital affiliated to Shanghai Jiaotong University, School of Medicine (Shanghai, China). A rat femur model was used and the surgical procedures were conducted under sterile conditions as previously described [32]. Briefly, the rats were anesthetized by intraperitoneal injection of ketamine (10 mg/kg). Each rat was immobilized with the knee joint in maximally flexed position and both legs were shaved and depilated. Afterwards, a longitudinal incision about 10 mm long was made along the lateral side of the extensor mechanism around the knee joint. With the knee in flexion, a cylindrical hole (2 mm in diameter) was drilled through the intercondylar notch and distal femoral metaphysis parallel to the long axis of the femur. The implants were placed bilaterally resulting in two implants per rat. The wound was closed carefully. Nine 12-week-old male Sprague Dawley rats (SD rats) were randomly divided into 3 groups corresponding to PEEK, Ta-30, and Ta-120. After surgery, the rats were housed in ventilated rooms and given access to water and food.

Table 2
Primer pairs used in real-time PCR analysis.

Gene	Primers (F = forward, R = reverse)	Amplicon
COL-I	F: CTGCCCAGAAGAATATGTATCACC R: GAAGCAAAGTTTCCTCCAAGACC	198 bp
Runx2	F: TCTTCCCAAAGCCAGAGCG R: TGCCATTCGAGGTGGTCG	154 bp
BMP-2	F: TGGGTTTGTGGTGGAAGTGGC R: TGGATGTCCTTTACCGTCGTG	154 bp
ALP	F: CGTCTCCATGGTGGATTATGCT R: CCCAGGCACAGTGGTCAAG	209 bp
OCN	F: GCCCTGACTGCATTCTGCCTCT R: TCACCACCTTACTGCCCTCCTG	103 bp
OPN	F: CCAAGCGTGGAAACACACAGCC R: GGCTTTGGAACTCGCCTGACTG	165 bp
β-actin	F: CACCCGCGAGTACAACCTTC R: CCCATACCCACCATCACACC	207 bp

2.4.2. Sequential fluorescent labeling

To characterize the new bone formation and mineralization, a polychrome sequential fluorescent labeling method was used. At 2, 4, and 6 weeks after operation, different fluorochromes were administered intraperitoneally at a sequence of 30 mg/kg alizarin red S (Sigma–Aldrich, USA), 25 mg/kg tetracycline hydrochloride (Sigma–Aldrich), and 20 mg/kg calcein (Sigma–Aldrich), respectively.

2.4.3. Sample preparation

The rats were sacrificed after 8 weeks post-implantation. The femurs with the implants were harvested and fixed in 10% buffered formaldehyde for micro-CT assay and histomorphometric observation.

2.4.4. Micro-CT assay

The fixed samples were imaged by micro-CT (SkyScan 1176, Bruker, USA) to determine the newly formed bone. The scanning parameters were set at 65 kV using the Al 1 mm filter with a resolution of 18 μm. After scanning, the two-dimensional (2D) and three-dimensional (3D) models were reconstructed using the NRecon software (Skyscan, USA) and CTvol program (SkyScan) and the bone volume around the implant was determined using the DataViewer software (SkyScan) and CTAn program (SkyScan).

2.4.5. Histological evaluation

After micro-CT, six femur specimens of each group were dehydrated by ascending concentrations of ethanol and embedded in polymethylmethacrylate (PMMA). The embedded specimens were cut into 150 μm thick sections perpendicular to the bone using a Leica SP1600 saw microtome (Leica, Hamburg, Germany) and polished to a final thickness of about 50 μm for fluorescence labeling observation under the confocal laser scanning microscope (Leica SP8, Hamburg, Germany). The excitation/emission wavelengths used to observe chelating fluorochromes were 543/620 nm, 405/575 nm and 488/520 nm for alizarin red S (red), tetracycline hydrochloride (yellow) and calcein (green), respectively.

After fluorescence microscopy, the same sections were counter-stained Van Gieson's picrofuchsin and examined to visualize the mineralized bone tissue (red). The images were captured by a fluorescence microscope (Olympus IX 71, Olympus, Japan) and the panoramic images were acquired by the Multiple Image Alignment (MIA) process. Histomorphometric analysis to evaluate the percentage of bone-implant contact (BIC) was performed on the same sections of each group. All the areas of interest were within the endosseous part of each implant and randomly picked. The images were analyzed using the Image-Pro Plus 6.0 software.

2.5. Statistical analysis

All the data were expressed as means ± standard deviation (SD). Statistically significant differences (p) between groups were measured using the one-way analysis of the variance and Tukey's multiple comparison tests. All the statistical analyses were determined with the GraphPad Prism 5 statistical software package. The difference were considered statistically significant at $^{*}p < 0.05$, $^{**}p < 0.01$, and $^{***}p < 0.001$.

3. Results

3.1. Surface characterization

The surface of the PEEK samples before and after Ta-PIII is shown in Fig. 1. The untreated PEEK (Fig. 1a) has a relatively flat and smooth surface with the exception of a few scratches due to pre-polishing. After Ta-PIII, nanoparticles with different sizes are homogeneously and densely distributed on both Ta-30 and Ta-120 as shown in Fig. 1b and c. According to the high magnification images in the inset, the size of nanoparticles on Ta-120 is around 20 nm, which is larger than that on Ta-30 (3–5 nm).

The XPS spectra are displayed in Fig. 2. In comparison with the XPS full spectrum of PEEK (Fig. 2a), characteristic peaks of Ta 4f, Ta 4d5/2, and Ta 4p3/2 are detected from Ta-30 and Ta-120 (Fig. 2b and c). According to the high-resolution spectra of Ta 4f (inserted images), the peaks at 24.7 eV and 26.7 eV from both Ta-30 and Ta-120 correspond to the typical binding energy of Ta_2O_5 [33], indicating that the nanoparticles on the Ta-PIII surfaces are stable and oxidized after exposure to air. No other elements are detected from both modified samples suggesting a clean surface after Ta-PIII. According to the XPS depth profiles of Ta in Fig. 2d, the amount

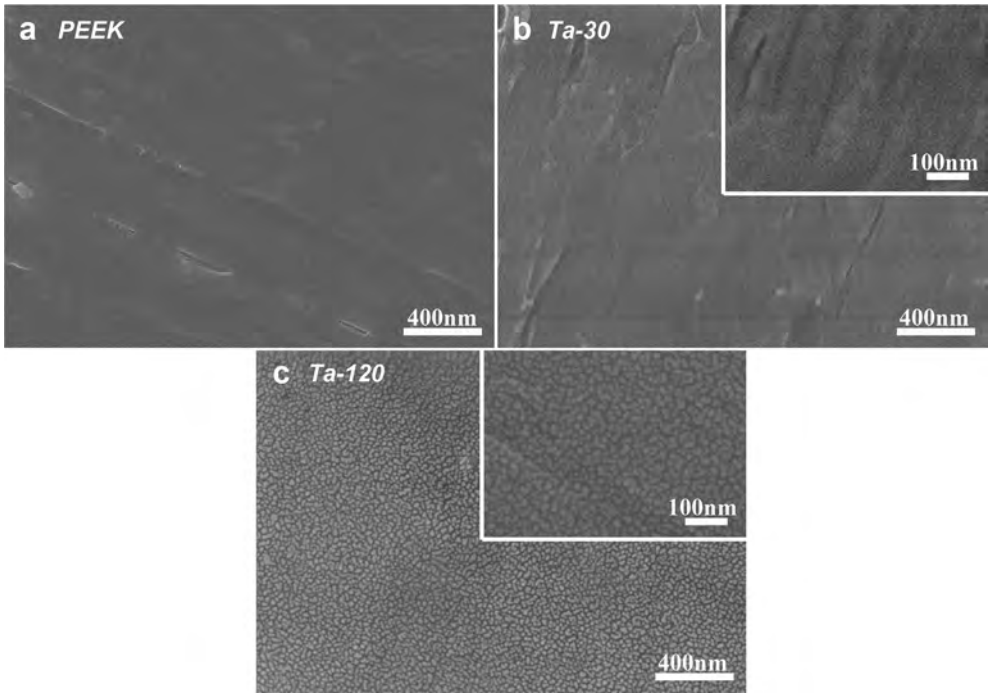

Fig. 1. Surface morphology of the samples: (a) PEEK; (b) Ta-30; (c) Ta-120. The inset at the top right corner in (b or c) is the high-magnification picture of each sample (100,000 ×).

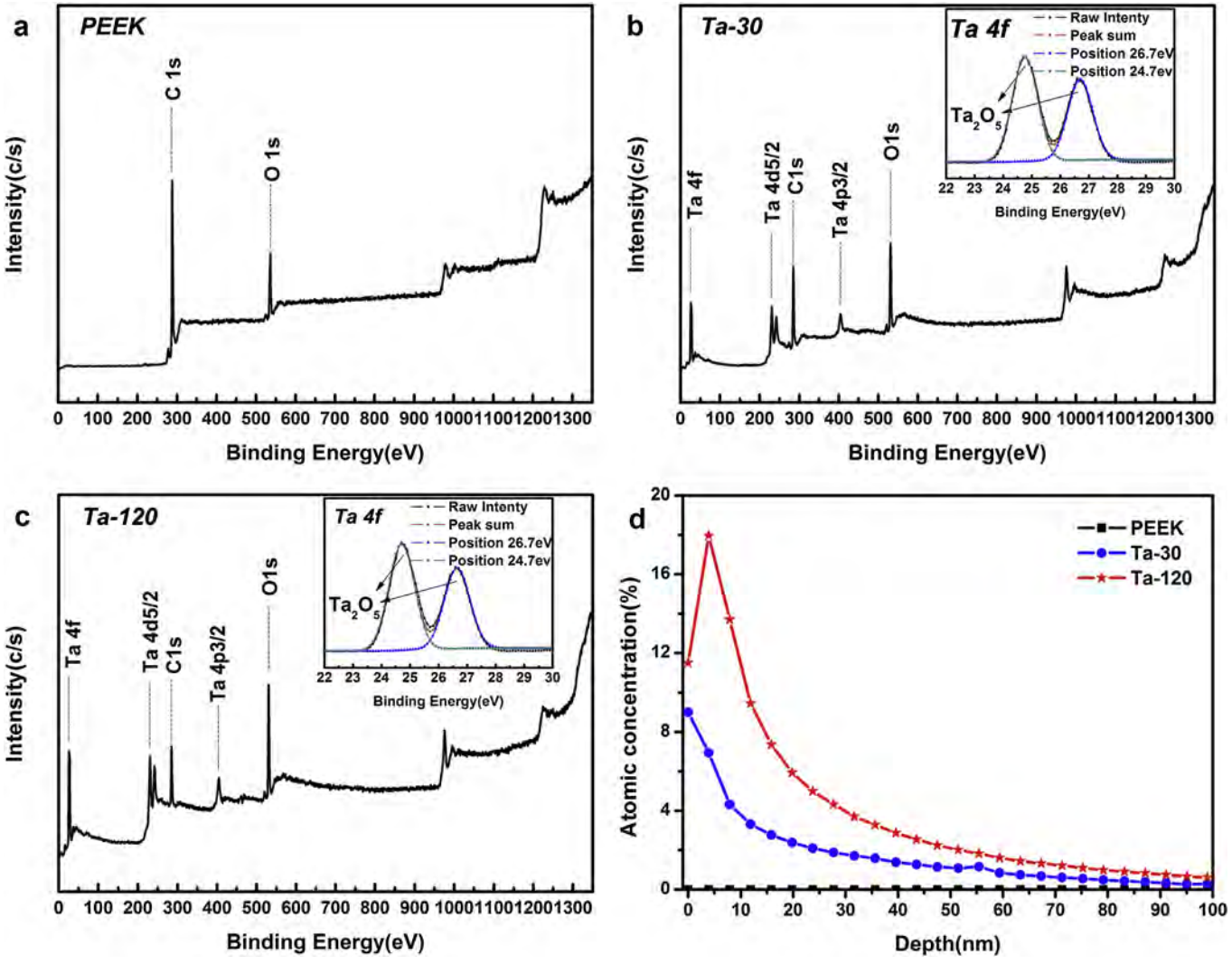

Fig. 2. XPS full and high-resolution spectra obtained from the samples: (a) PEEK; (b) Ta-30; (c) Ta-120; (d) XPS depth profiles of Ta. The insets at the top right corner in (b and c) are high-solution spectra of Ta 4f for the samples.

of Ta increases with implantation time. The Ta peak of Ta-30 (about 9 atomic %) is in the outer layer, whereas that of Ta-120 (about 18 at %) is at a depth of 5 nm. The depth profile of Ta-120 resembles a Gaussian distribution.

The elastic modulus and nanohardness values as a function of indentation depths from 20 nm to 100 nm are depicted in Fig. 3a and b, respectively. The nanohardness increases from 0.9 GPa to 2.3 GPa and the elastic modulus increases from 5.5 GPa to 9.5 GPa after Ta-PIII. The load–displacement curves are shown in Fig. 3c. All the curves are continuous during the test indicating no abrupt cracking of the Ta-PIII modified layers. At the same load of 1.3 mN and compared to PEEK, the indentation depths of the Ta-PIII samples are smaller and the elastic recovery is larger, suggesting better elastic resistance after Ta-PIII.

3.2. Response of bMSCs in vitro

3.2.1. Cell adhesion and cell proliferation

Among the various types of cells, marrow-derived bone mesenchymal stem cells (bMSCs), which possess the critical properties in osteointegration rendering them suitable for bone tissue engineering applications, are considered the ideal cells for the evaluation of osteogenic properties of bone substitutes. The initial adhesion behavior and spreading activity of bMSCs are monitored by SEM at different time points, as shown in Fig. S1. The bMSCs on the PEEK surface exhibit a spherical morphology within the initial three hours after seeding, but those on Ta-30 and Ta-120 surfaces show apparent filopodia and lamellipodia extensions. After culturing for 24 h, the bMSCs attach and spread well on all the surfaces. The cluster cells are interconnected by a large number of filopodia, especially Ta-30 on which the cells nearly cover the whole surface, indicating that Ta-PIII alters the initial cellular adhesion of bMSCs.

The time-related proliferation of bMSCs is evaluated by the alamarBlue™ assay and the data are presented in Fig. 4a. After culturing for 1 day, proliferation of bMSCs on Ta-30 is statistically higher ($p < 0.01$) than that on PEEK and the trend is in accordance with the adhesion results. On the other hand, bMSC proliferation on Ta-120 shows no statistical difference compared to either PEEK or Ta-30. When the culturing time is extended to 4 and 7 days, the number of bMSCs on the Ta-PIII samples is larger than that on PEEK and the statistical difference becomes more significant ($p < 0.001$), indicating that Ta-PIII is more advantageous to bMSC proliferation and induces no apparent toxicity to the bMSCs.

3.2.2. ALP activity

Fig. 4b shows the qualitative and quantitative *ALP* expressions of bMSCs on the samples. The *ALP*-positive areas are stained and shown in Fig. S2. The *ALP*-positive areas are obviously larger on Ta-30 and Ta-120 than on PEEK after culturing for 7 days. After 14 days,

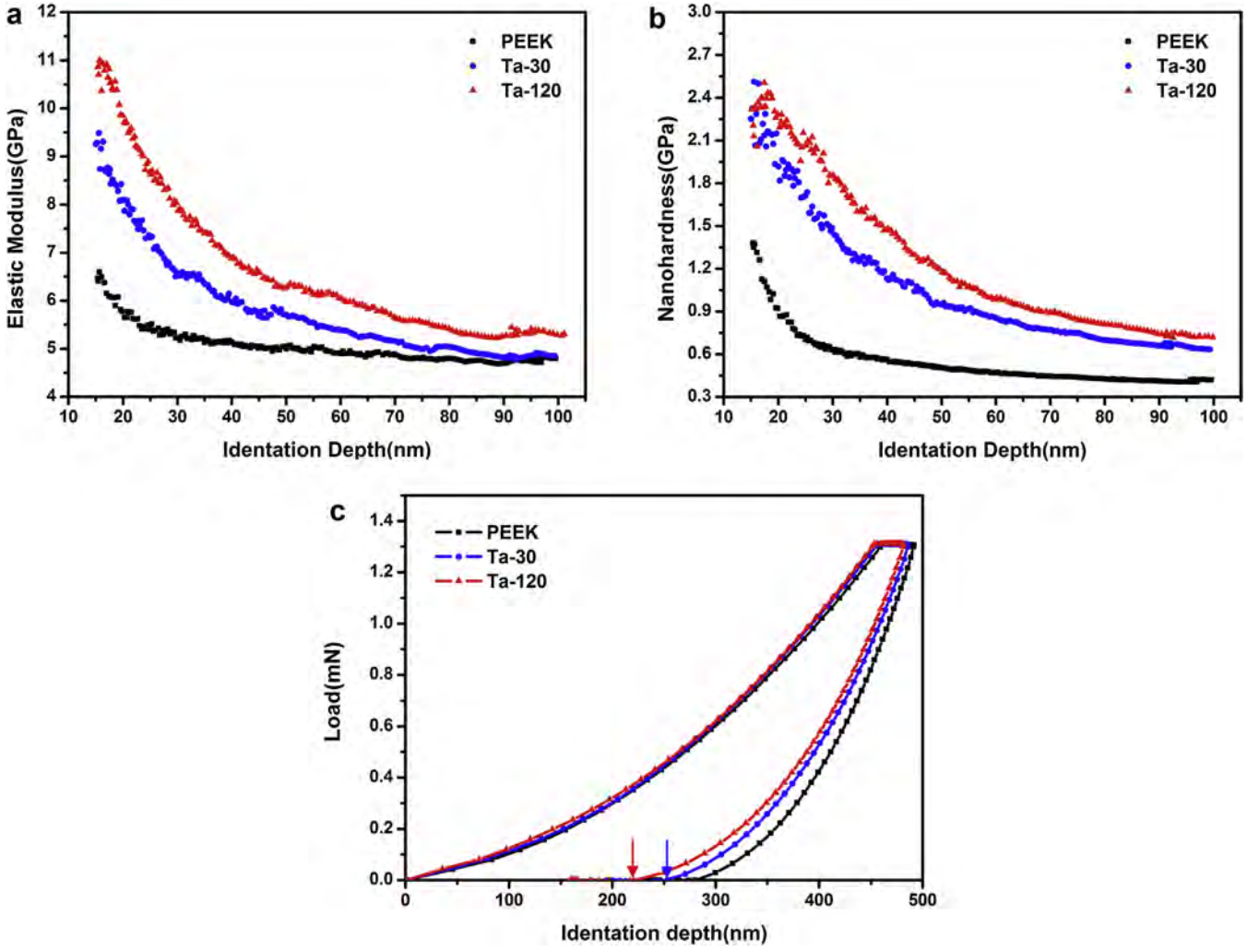

Fig. 3. (a) Elastic modulus, (b) Nanohardness, and (c) Load–displacement curves of all samples at indentation load of 1.3 mN.

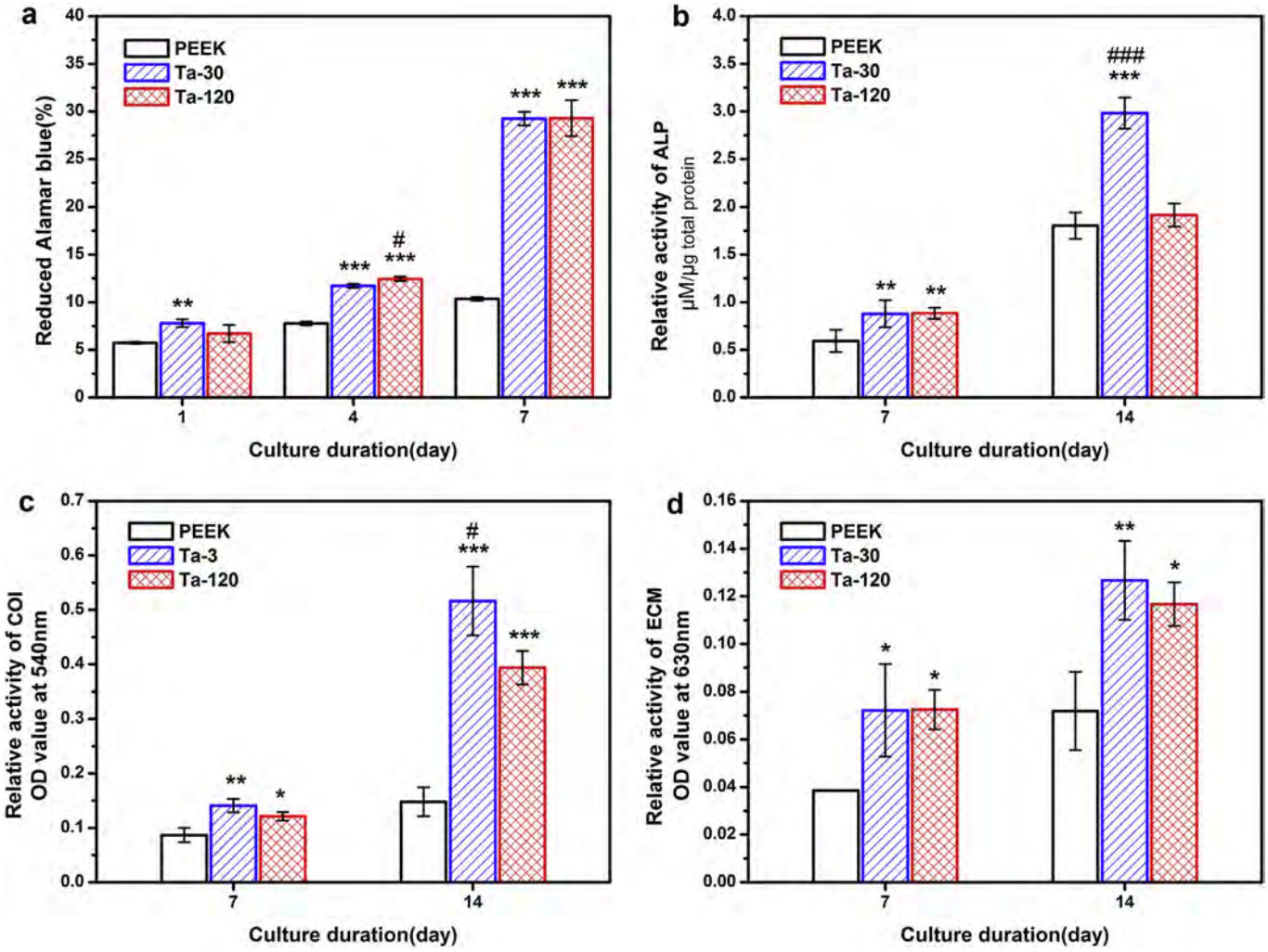

Fig. 4. (a) Reduction percentage of alamarBlue™ for bMSCs cultured on the samples for 1, 4 and 7 days. (b) *ALP* activity assay of the bMSCs cultured on the samples for 7 and 14 days. (c) *COL* secretion assay of bMSCs cultured on the samples for 7 and 14 days. (d) *ECM* mineralization assay of bMSCs cultured on the samples for 7 and 14 days. *($p < 0.05$), **($p < 0.01$), ***($p < 0.001$) when compared with PEEK; #($p < 0.05$), ###($p < 0.001$) when compared with Ta-120.

more *ALP* is generated on the Ta-30 surface. The results are corroborated by the quantitative analysis, suggesting the long-term stimulating effects of *ALP* activity on Ta-30.

3.2.3. Collagen secretion

Collagen secretion of bMSCs quantified by the sirius red staining method is shown in Fig. 4c. According to stained images (Fig. S3), more collagen is secreted on the Ta-PIII surface than PEEK. Besides, Ta-30 can induce much denser collagen deposition of bMSCs than Ta-120 and this trend becomes more significant as the culturing time is extended to 14 days.

3.2.4. Extracellular matrix mineralization

Extracellular matrix (*ECM*) mineralization of bMSCs determined by alizarin red staining is shown in Fig. 4d. According to the *ECM* staining images (Fig. S4), small calcium nodes marked by blue arrows appear on the Ta-PIII samples after culturing for 7 days. The number of calcium nodes increases and the size becomes bigger when the culturing time is extended to 14 days, as marked by the white arrows. After 14 days, the bMSCs exhibit slightly up-regulated *ECM* mineralization on Ta-30 compared to Ta-120, as shown by the quantitative analysis.

3.2.5. Osteogenesis-related gene expressions

To investigate the bMSC differentiation on the surface, the expressions of six typical osteogenesis-related genes including *COL-I*, *Runx2*, *BMP-2*, *ALP*, *OCN* and *OPN* are quantified by real-time PCR (Fig. 5). The results are normalized to β-actin and expressed as relative expression levels to the untreated PEEK. In general, the bMSCs cultured on Ta-PIII samples exhibit higher gene expressions. In the early stage (after culturing for 7 days), the gene expression of *COL-I* ($p < 0.01$) and *ALP* ($p < 0.05$) on Ta-30 is significantly higher, while expressions of *OCN* ($p < 0.05$) and *OPN* ($p < 0.001$) are significantly promoted on Ta-30 in the later stage (14 days). *COL-I* and *ALP* are considered as the early markers and *OCN* and *OPN* as the later markers for osteogenic differentiation. Therefore, our results indicate that Ta-30 enhances osteogenic differentiation of bMSCs at all time.

3.3. In vivo osteointegration of implant surface

3.3.1. Micro-CT evaluation of bone formation

Fig. 6 shows the 2D and 3D images reconstructed by Micro-CT. The 2D images of coronal sections along the central axis of PEEK, Ta-30, and Ta-120 are depicted in Fig. 6d, e, and f, respectively. Cancellous bones inside the marrow cavity are marked by green

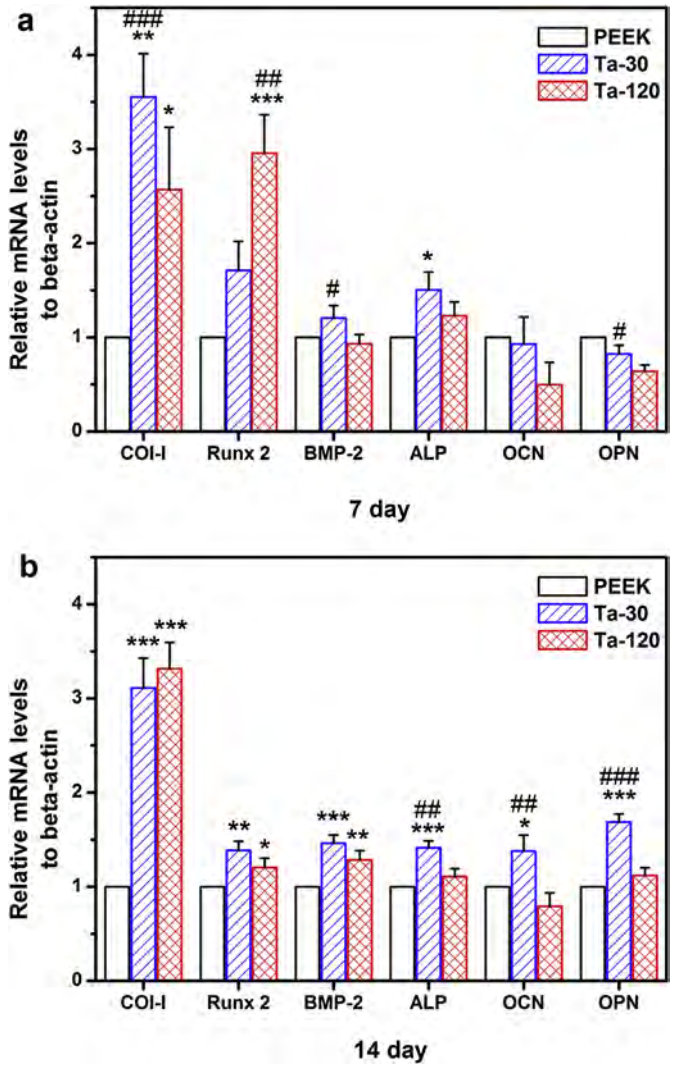

Fig. 5. Real-time PCR detection of osteogenesis-related gene expression of the bMSCs cultured on the samples for 7 and 14 days. *($p < 0.05$), **($p < 0.01$) and ***($p < 0.001$) when compared with PEEK; #($p < 0.05$), ##($p < 0.01$) and ###($p < 0.001$) when compared with Ta-120.

rectangles and more bones are found in the marrow cavity of the Ta-PIII samples. The bone volume around the implant surfaces in the marrow cavity of the Ta-PIII samples is larger than that of PEEK and the bone volume around Ta-30 is the largest among the three groups. The reconstructed 3D images of PEEK, Ta-30, and Ta-120 are presented in Fig. 6g, h, and i, respectively. More new bone forms on the Ta-PIII samples consistent with the 2D images.

3.3.2. Sequential fluorescent labeling analysis

Sequential fluorescent labeling (for 8 weeks) is used to record and monitor new bone formation around the three implant groups by applying three types of fluorochromes. As shown in Fig. 7d, the rectangular region adjacent to each implant surface is imaged. After 2 weeks, alizarin red is found to be deposited and layered on all three surfaces (Fig. 7a~c). However, at subsequent time points (4 weeks and 6 weeks), tetracycline (yellow) and calcein (green) can hardly be found from the PEEK surface. On the contrary, distinctive yellow and green fluorescent lines can be observed from the Ta-PIII samples (Fig. 7b and c), indicating that the Ta incorporated PEEK promotes new bone formation. The percentage of the area of three fluorochromes stained bone is calculated and shown in Fig. 7e. The percentage of fluorescent labeling area on Ta-30 (13.91 ± 4.08%) is significantly larger than those on PEEK (3.29 ± 0.92%, $p < 0.01$) and Ta-120 (6.32 ± 0.77%, $p < 0.05$). All in all, sequential fluorescent labeling indicates that Ta-PIII stimulates more new bone formation at every time points, especially Ta-30.

3.3.3. Histological observation and analysis

The histological sections (8 weeks post-implantation) processed by Van Gieson's picrofuchsin staining are shown in Fig. 8. The MIA images (Fig. 8a–1, b-1, and c-1) exhibit the full views of the bone formation situation around PEEK, Ta-30, and Ta-120, respectively. More newly formed bone can be observed after Ta-PIII, especially Ta-30. At a large magnification (40×), the bone layer on PEEK is discontinuous (Fig. 8a-2) but those on the Ta-PIII samples (Fig. 8b-2 and c-2) are intact and much thicker at the same section of implants, especially Ta-30 (Fig. 8b-2). The image at a larger magnification (Fig. 8a-3, 200 ×) reveals that fibrous connective tissues (blue) are formed around the PEEK implant and separate the bone tissues from the implant (marked by green arrows). This phenomenon is not observed from the Ta-PIII implants (Fig. 8b-3 and c-3) on which the bone layers bond tightly and directly (marked by white arrows). The bone-implant contact (BIC) is measured from six different specimens of each group and the results are presented in Fig. S5. The BIC index of Ta-30 is 54.89 ± 3.13% that is significantly larger than that of both Ta-120 (39.94 ± 2.41%, $p < 0.001$) and PEEK (19.60 ± 6.17%, $p < 0.001$), suggesting the Ta-30 induces the best bone-implant contact among the three groups.

4. Discussion

In this work, PEEK is plasma implanted with Ta to enhance osteointegration and as confirmed by XPS (Fig. 2a~c), different amounts of tantalum are introduced by Ta-PIII. No obvious Ta release is observed from the samples (Table 3) after immersing in PBS for 28 days, confirming the robustness of the modified surfaces perhaps arising from the stable Ta_2O_5. Unlike coating techniques, Ta-PIII does not create a distinct boundary between the modified layer and substrate (Fig. 2d) and concern over delamination is minimized. Nanoindentation tests indicate that Ta-PIII raises the elastic modulus of PEEK from 5.5 GPa to 9.5 GPa and nanohardness from 0.9 GPa to 2.4 GPa (Fig. 3a and b) and the Ta-PIII samples exhibit better elastic recovery as well (Fig. 3c). The elastic modulus of human cancellous bone ranges from 1.3 GPa to 7.8 GPa while that of cortical bone ranges from 12 GPa to 20 GPa [34,35]. Hence, the Ta-PIII PEEK samples possess surface elastic moduli more similar to cortical bone thus boding well for osteointegration.

PIII is a low temperature plasma technique suitable for heat-sensitive polymeric materials. In PIII, by applying negative voltage pulses, the sample is implanted with energetic ions generated from a cathodic arc [30] and thermal energy is generated by atomic scale heating (ASH) [29,36]. It has been suggested that ASH can replace conventional heating to produce dense films on substrates at a low temperature [37,38]. In our experiments, the PEEK samples are implanted with Ta ions at a high voltage of 30 kV and small nanoparticle islands are formed on the Ta-30 surface (Fig. 1b). This probably explains why the condensing tantalum does not wet the PEEK surface. As PIII proceeds, larger islands are formed (Fig. 1c) due to the heat accumulation gradually reaching the state of thermodynamic equilibrium [36,39]. In addition to the produced nanostructure, energetic condensation of the Ta plasma alters the surface elastic modulus and hardness. Owing to the relatively poor thermal conductivity, the thermal effects on the PEEK surface is magnified by heat accumulation to induce carbonization, cross-linking, or even fusion and resolidification of the surface [40–42]. It

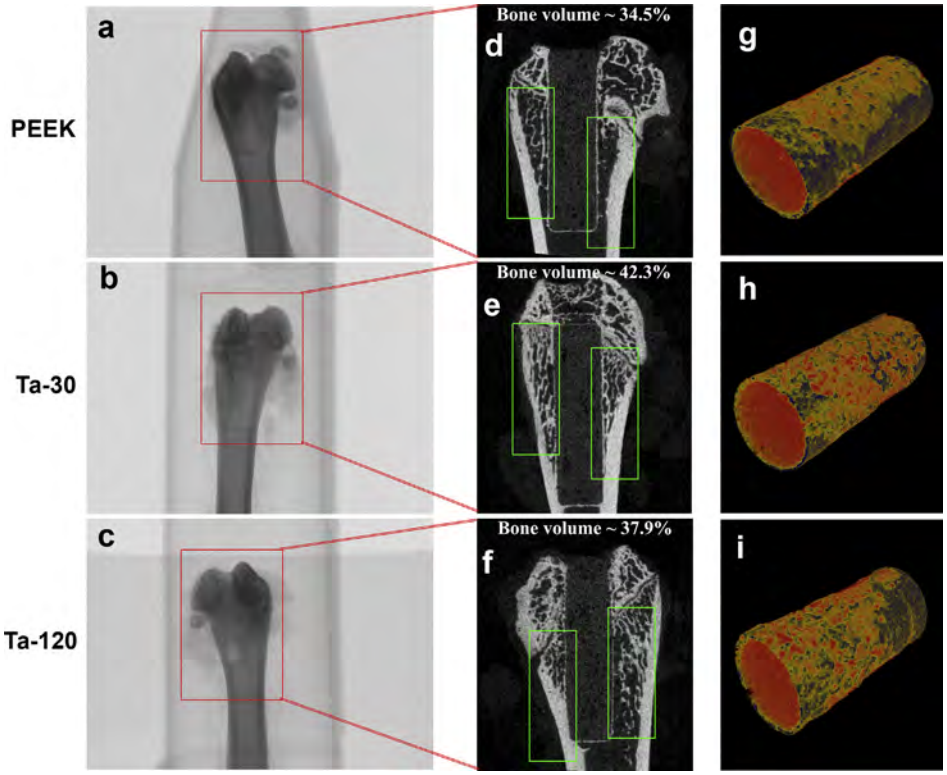

Fig. 6. Characterization of implants and the surrounding bones by Micro-CT. The full and corresponding 2D coronal section views of rat femur bones with implants inside: (a and d) PEEK; (b and e) Ta-30; (c and f) Ta-120. Reconstructed 3D models of (g) PEEK, (h) Ta-30 and (i) Ta-120 implants.

should be noted that the variation in the elastic modulus and nanohardness is consistent with the Ta depth profile, indicating that the amount of Ta contributes to the alteration in the surface mechanical characteristics. Our results suggest that the thermal effects *via* ASH and incorporation of tantalum synergistically alter the surface elastic modulus and nanohardness of PEEK.

Specific differentiation of bMSCs can be tailored by altering the surface properties of the biomaterials such as the surface chemical composition, structure, and mechanical properties [21,43]. As presented above, tantalum incorporation, nanostructure fabrication, and enhanced surface mechanical properties are simultaneously achieved on PEEK by Ta-PIII. To investigate the influence of surface

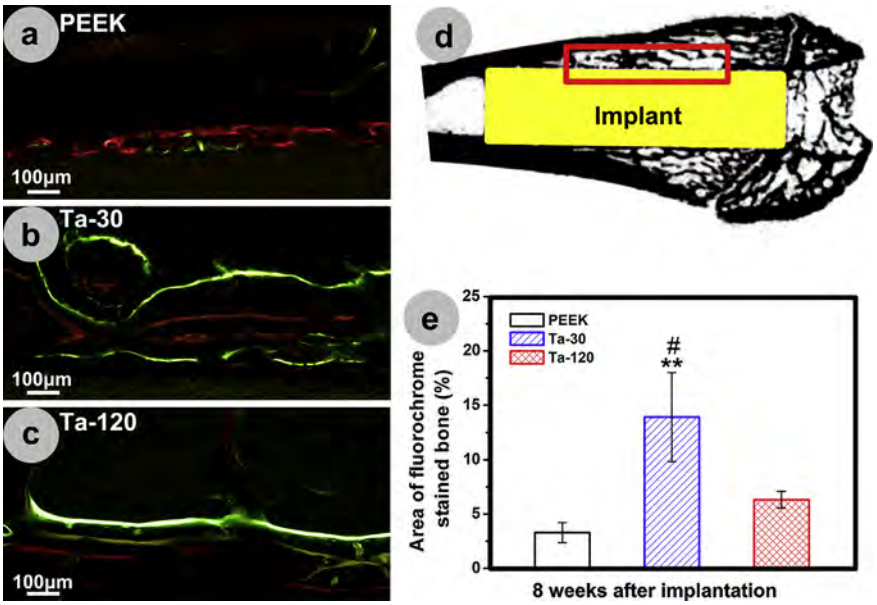

Fig. 7. Sequential fluorescent labeling observation: (a) PEEK, (b) Ta-30, and (c) Ta-120. Red, yellow and green represent labeling by alizarin red S, tetracycline hydrochloride and calcein, respectively. (d) Illustration of selected area to evaluate new bone formation process. (e) Histogram of percentage for the area of fluorochromes stained bone. $^{**}(p < 0.01)$ when compared with PEEK; $\#(p < 0.05)$ when compared with Ta-120. (For interpretation of the references to color in this figure legend, the reader is referred to the web version of this article.)

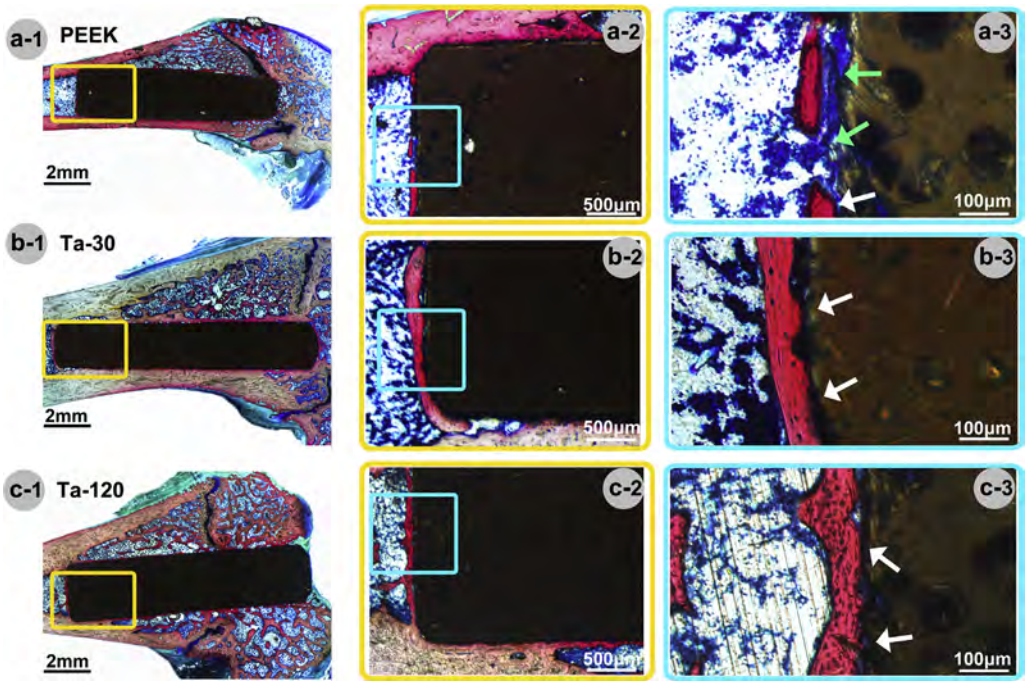

Fig. 8. Histological observations. MIA images are shown at low magnification and the insets are shown at high magnification. Images (magnification 40×) of yellow rectangular marked areas are shown in (a-2) PEEK, (b-2) Ta-30 and (c-2) Ta-120, respectively. Images (magnification 200×) of cyan rectangular marked areas are shown in (a-3) PEEK, (b-3) Ta-30 and (c-3) Ta-120, respectively. White arrows marked the direct contact between implants and new bones. Green arrows marked the fibrous tissue covering area. (For interpretation of the references to color in this figure legend, the reader is referred to the web version of this article.)

properties on osteointegration of PEEK materials, both *in vitro* and *in vivo* studies are conducted. Adhesion and proliferation of bMSC are improved after Ta-PIII (Fig. S1 and Fig. 4a) and the good cytocompatibility of Ta is also confirmed. *ALP* activity, *COL* secretion, *ECM* mineralization, and osteogenesis-related gene expressions of bMSCs are qualitatively and quantitatively measured to assess osteogenic differentiation of bMSCs *in vitro*. In general, bMSCs on the two Ta-PIII surfaces exhibit a stronger osteogenic differentiation tendency on both the molecular and genetic levels (Fig. 4b~d and Fig. 5). *ECM* plays the key role when bMSCs sense and respond to the stiffness of the materials surface. By altering the density or organization components of the *ECM* such as collagen, the stem cell fate can be affected. Engler et al. have disclosed that bMSCs are capable of driving themselves to osteogenic differentiation on a stiff matrix probably *via* adjusting deformation of *ECM* according to the matrix elasticity [44]. According to our results, *ECM* mineralization of bMSCs on both Ta-PIII samples is significantly enhanced compared to PEEK and this trend becomes more significant as the culturing time becomes longer (Fig. 4d). Hence, it can be inferred that the microenvironment on the Ta-PIII samples is more beneficial to bMSC osteogenic differentiation due to the more similar elastic modulus to that of human native cortical bones. On the other hand, cell adhesion and proliferation of bMSCs on Ta-30 and Ta-120 show no apparent difference, but the bMSCs on Ta-30 exhibit significantly higher osteogenic activity than Ta-120. It has been reported that the formation of Ta–OH on tantalum contributes to its bioactivity [45,46]. Besides, smaller Ta_2O_5 nanoparticles possess a larger specific surface area and higher activity to generate Ta–OH groups. Therefore, more collagen fibrils and calcium nodes are deposited and formed on the Ta-30 surface. These appear to be the main reasons for the excellent osteogenic activity of bMSCs observed from Ta-30 but more studies are needed to elucidate the accurate mechanism.

Since biomaterials often perform differently *in vitro* and *in vivo*, animal tests are conducted in this work to evaluate osteointegration *in vivo*. A rat femur implantation model is adopted here. The implants are inserted in the cortico-cancellous bones of the femoral marrow cavity where bMSCs exist abundantly. After 8 weeks, the Ta-PIII samples exhibit superior osteointegration by stimulating the growth of more new bone both on the surface and in the cavity, as shown by the 3D models and 2D images acquired from micro-CT (Fig. 6). Sequential fluorescent labeling results reveal the new bone formation process (Fig. 7), further confirming better osteointegration after Ta-PIII. It is noted that new bone formation on the PEEK surface is substantial only in the early stage after implantation, but that on the Ta-PIII samples can be observed throughout the entire examination period. Histological observation (Fig. 8) and BIC analysis (Fig. S5) show that new bones are formed surrounding the entire implants for both Ta-30 and Ta-120. In the areas where the implants are in contact with native cortical bones, the new bone forms well and can grow along the implants thus confirming excellent osteoconductivity on the modified PEEK

Table 3
Ta ion concentration in PBS after immersion for different time.

Immersion period (days)		0~7	7~14	14~21	21~28
Ta ion concentration (μg/mL)	Ta-30	0.017	Undetected	Undetected	Undetected
	Ta-120	Undetected	Undetected	Undetected	Undetected

Undetected: Ta ion concentration below 0.002 μg/mL.

surfaces. On the contrary, in the areas where implants are far from the cortical bones and exposed to the bMSCs in the cavity, evident fibrous tissues are found between the implant and bone on the untreated PEEK control. The new bones make direct contact with Ta-30 and Ta-120, indicating that the bMSCs exhibit osteo-differentiation on the Ta-PIII surfaces. The results suggest that the modified surfaces with a similar elastic modulus to native bone possess good osteoinductivity as well. The movies (Movie 1, 2 and 3) showing bone formation around the implants (PEEK, Ta-30 and Ta-120) are available in the supporting materials for confirmation and the *in vivo* and *in vitro* presented here are consistent and positive.

Supplementary video related to this article can be found at http://dx.doi.org/10.1016/j.biomaterials.2015.02.018.

5. Conclusion

PEEK surfaces are plasma implanted with tantalum to improve its surface mechanical properties and osteogenic activity. The mechanical properties after Ta PIII, for instance, the elastic modulus, nanohardness, and elastic recovery are more favorable and in particular, the elastic modulus of the Ta-PIII PEEK samples is closer to that of human cortical bones than the untreated PEEK. The Ta-PIII PEEK surfaces also exhibit enhanced osteogenic differentiation of rat bMSCs *in vitro*. In a cortico-cancellous rat femur implantation model, faster and better osteointegration can be observed around the Ta-PIII implants *in vivo*. Our results reveal the significance of the surface elastic modulus for osteointegration both *in vitro* and *in vivo*. The surface modified PEEK materials are more suitable for orthopedic and dental applications and have large clinical potential.

Acknowledgments

Financial support from the National Basic Research Program of China (973 Program, 2012CB933600), Shanghai Committee of Science and Technology, China (14JC1493100 and 14XD1403900), National Natural Science Foundation of China (81271704), City University of Hong Kong Strategic Research Grant (SRG) No. 7004188, and Hong Kong Research Grants Council (RGC) General Research Funds (GRF) No. CityU 112212 are acknowledged.

Appendix A. Supplementary data

Supplementary data related to this article can be found at http://dx.doi.org/10.1016/j.biomaterials.2015.02.018.

References

[1] Geetha M, Singh AK, Asokamani R, Gogia AK. Ti based biomaterials, the ultimate choice for orthopaedic implants – a review. Prog Mater Sci 2009;54:397–425.
[2] Gentleman E, Swain RJ, Evans ND, Boonrungsiman S, Jell G, Ball MD, et al. Comparative materials differences revealed in engineered bone as a function of cell-specific differentiation. Nat Mater 2009;8:763–70.
[3] Navarro M, Michiardi A, Castano O, Planell JA. Biomaterials in orthopaedics. J R Soc Interface 2008;5:1137–58.
[4] Kurtz SM, Devine JN. PEEK biomaterials in trauma, orthopedic, and spinal implants. Biomaterials 2007;28:4845–69.
[5] Toth JM, Wang M, Estes BT, Scifert JL, Seim HB, Turner AS. Polyetheretherketone as a biomaterial for spinal applications. Biomaterials 2006;27:324–34.
[6] Sagomonyants KB, Jarman-Smith ML, Devine JN, Aronow MS, Gronowicz GA. The in vitro response of human osteoblasts to polyetheretherketone (PEEK) substrates compared to commercially pure titanium. Biomaterials 2008;29:1563–72.
[7] Ryan G, Pandit A, Apatsidis DP. Fabrication methods of porous metals for use in orthopaedic applications. Biomaterials 2006;27:2651–70.
[8] Chaneliere C, Autran JL, Devine RAB, Balland B. Tantalum pentoxide (Ta2O5) thin films for advanced dielectric applications. Mater Sci Eng R Rep 1998;22:269–322.
[9] Li Y, Zhao T, Wei S, Xiang Y, Chen H. Effect of Ta2O5/TiO2 thin film on mechanical properties, corrosion and cell behavior of the NiTi alloy implanted with tantalum. Mater Sci Eng C Mater Biol Appl 2010;30:1227–35.
[10] Wang N, Li H, Wang J, Chen S, Ma Y, Zhang Z. Study on the anticorrosion, biocompatibility, and osteoinductivity of tantalum decorated with tantalum oxide nanotube array films. Acs Appl Mater Interfaces 2012;4:4516–23.
[11] Matsuno H, Yokoyama A, Watari F, Uo M, Kawasaki T. Biocompatibility and osteogenesis of refractory metal implants, titanium, hafnium, niobium, tantalum and rhenium. Biomaterials 2001;22:1253–62.
[12] Niinomi M, Nakai M, Hieda J. Development of new metallic alloys for biomedical applications. Acta Biomater 2012;8:3888–903.
[13] Okazaki Y, Gotoh E. Comparison of metal release from various metallic biomaterials in vitro. Biomaterials 2005;26:11–21.
[14] Wang HF, Li J, Yang HL, Liu C, Ruan JM. Fabrication, characterization and in vitro biocompatibility evaluation of porous Ta-Nb alloy for bone tissue engineering. Mater Sci Eng C Mater Biol Appl 2014;40:71–5.
[15] Diomidis N, Mischler S, More NS, Roy M. Tribo-electrochemical characterization of metallic biomaterials for total joint replacement. Acta Biomater 2012;8:852–9.
[16] Cohen R. A porous tantalum trabecular metal: basic science. Am J Orthop (Belle Mead, NJ) 2002;31:216–7.
[17] Levine BR, Sporer S, Poggie RA, Della Valle CJ, Jacobs JJ. Experimental and clinical performance of porous tantalum in orthopedic surgery. Biomaterials 2006;27:4671–81.
[18] Liu H, Lin J, Roy K. Effect of 3D scaffold and dynamic culture condition on the global gene expression profile of mouse embryonic stem cells. Biomaterials 2006;27:5978–89.
[19] Welldon KJ, Atkins GJ, Howie DW, Findlay DM. Primary human osteoblasts grow into porous tantalum and maintain an osteoblastic phenotype. J Biomed Mater Res Part A 2008;84A:691–701.
[20] Liu X, Chu PK, Ding C. Surface nano-functionalization of biomaterials. Mater Sci Eng R Rep 2010;70:275–302.
[21] Nel AE, Madler L, Velegol D, Xia T, Hoek EMV, Somasundaran P, et al. Understanding biophysicochemical interactions at the nano-bio interface. Nat Mater 2009;8:543–57.
[22] Chu PK. Recent applications of plasma-based ion implantation and deposition to microelectronic, nano-structured, and biomedical materials. Surf Coat Technol 2010;204:2853–63.
[23] Chu PK. Applications of plasma-based technology to microelectronics and biomedical engineering. Surf Coat Technol 2009;203:2793–8.
[24] Wang H, Kwok DTK, Xu M, Shi H, Wu Z, Zhang W, et al. Tailoring of mesenchymal stem cells behavior on plasma-modified polytetrafluoroethylene. Adv Mater 2012;24:3315–24.
[25] Wang H, Xu M, Zhang W, Kwok DTK, Jiang J, Wu Z, et al. Mechanical and biological characteristics of diamond-like carbon coated poly aryl-ether-ether-ketone. Biomaterials 2010;31:8181–7.
[26] Bax DV, McKenzie DR, Weiss AS, Bilek MMM. The linker-free covalent attachment of collagen to plasma immersion ion implantation treated polytetrafluoroethylene and subsequent cell-binding activity. Biomaterials 2010;31:2526–34.
[27] Wang H, Lu T, Meng F, Zhu H, Liu X. Enhanced osteoblast responses to poly ether ether ketone surface modified by water plasma immersion ion implantation. Colloids Surf B Biointerfaces 2014;117:89–97.
[28] Lu T, Liu X, Qian S, Cao H, Qiao Y, Mei Y, et al. Multilevel surface engineering of nanostructured TiO2 on carbon-fiber-reinforced polyetheretherketone. Biomaterials 2014;35:5731–40.
[29] Anders A. Atomic scale heating in cathodic arc plasma deposition. Appl Phys Lett 2002;80:1100–2.
[30] Anders A. Metal plasma immersion ion implantation and deposition: a review. Surf Coat Technol 1997;93:158–67.
[31] Powles RC, McKenzie DR, Meure SJ, Swain MV, James NL. Nanoindentation response of PEEK modified by mesh-assisted plasma immersion ion implantation. Surf Coat Technol 2007;201:7961–9.
[32] Qiao Y, Zhang W, Tian P, Meng F, Zhu H, Jiang X, et al. Stimulation of bone growth following zinc incorporation into biomaterials. Biomaterials 2014;35:6882–97.
[33] McGuire GE, Schweitz Gk, Carlson TA. Study of core electron binding-energies in some group IIIA, VB, and VIB compounds. Inorg Chem 1973;12:2450–3.
[34] Rho JY, Kuhn-Spearing L, Zioupos P. Mechanical properties and the hierarchical structure of bone. Med Eng Phys 1998;20:92–102.
[35] Morgan EF, Bayraktar HH, Keaveny TM. Trabecular bone modulus-density relationships depend on anatomic site. J Biomech 2003;36:897–904.
[36] Anders A. Metal plasmas for the fabrication of nanostructures. J Phys D Appl Phys 2007;40:2272–84.
[37] Musil J. Hard and superhard nanocomposite coatings. Surf Coat Technol 2000;125:322–30.
[38] Musil J, Kunc F, Zeman H, Polakova H. Relationships between hardness, Young's modulus and elastic recovery in hard nanocomposite coatings. Surf Coat Technol 2002;154:304–13.
[39] Stepanov AL. Applications of ion implantation for modification of TiO2: a review. Rev Adv Mater Sci 2012;30:150–65.
[40] Gan BK, Bilek MMM, Kondyurin A, Mizuno K, McKenzie DR. Etching and structural changes in nitrogen plasma immersion ion implanted polystyrene

films. Nucl Instrum Methods Phys Res Sect B Beam Interact Mater Atoms 2006;247:254–60.
[41] Kondyurin A, Nosworthy NJ, Bilek MMM. Attachment of horseradish peroxidase to polytetrafluorethylene (teflon) after plasma immersion ion implantation. Acta Biomater 2008;4:1218–25.
[42] Shi W, Li XY, Dong H. Improved wear resistance of ultra-high molecular weight polyethylene by plasma immersion ion implantation. Wear 2001;250:544–52.
[43] Discher DE, Mooney DJ, Zandstra PW. Growth factors, matrices, and forces combine and control stem cells. Science 2009;324:1673–7.
[44] Engler AJ, Sen S, Sweeney HL, Discher DE. Matrix elasticity directs stem cell lineage specification. Cell 2006;126:677–89.
[45] Kokubo T, Kim HM, Kawashita M. Novel bioactive materials with different mechanical properties. Biomaterials 2003;24:2161–75.
[46] Miyazaki T. Development of bioactive materials based on bone-bonding mechanism on metal oxides. J Ceram Soc Jpn 2008;116:260–4.